Supporting Information

Dual Atomic Defect Modulation in Three-Dimensional Mesoporous Graphene for High-Performance Potassium Ion Hybrid Capacitors

Yize Wang,‡[a], Wenda Qiu,*‡[b,c] Peijun Deng,[a] Jing Fu,[a] Guoxian Li,[a] Chunjin Li,[a] Mingzu Zhang,[b] Pingji Yu,[b] Huajie Feng,*[a] and Xihong Lu[c]

[a] *Key Laboratory of Electrochemical Energy Storage and Energy Conversion of Hainan Province, Hainan Normal University, Haikou 571158, Hainan, China*

[b] *Guangdong Industry Polytechnic University, Guangzhou 510300, Guangdong, China*

[c] *MOE of the Key Laboratory of Bioinorganic and Synthetic Chemistry, KLGHEI of Environment and Energy Chemistry, School of Chemistry, Sun Yat-Sen University, Guangzhou 510275, Guangdong, China*

***Corresponding Author.**

E-mail: qiuwd3@mail3.sysu.edu.cn (W.D. Qiu), Fenghuajiehk@163.com (H.J. Feng)

‡Yize Wang and Wenda Qiu contributed equally to this work.

Calculations:

Specific capacities (C_{cell-s}) of half-cells and PIHCs devices were estimated from the discharge curve using the following equations:

$$C_{cell-s} = \frac{\int_{0}^{\Delta t} I \times dt}{m} \tag{1}$$

where $C_{cell\text{-}s}$ (mA h g^{-1}) is the specific capacity of the half-cells and PIHCs devices, I (mA) is the applied discharging current, Δt (h) is the discharging time and m (g) is the mass of the active material.

Specific energy density E and specific power density P of PIHCs devices were obtained from the following equations:

$$E = C_{cell-s} * \Delta V \tag{2}$$

$$P = \frac{C_{cell-s} * \Delta V}{\Delta t} \tag{3}$$

where E (Wh kg^{-1}) is the energy density, $C_{cell\text{-}s}$ is the specific capacity obtained from Equation (1) and ΔV (V) is the voltage window. P (W kg^{-1}) is the specific power density and Δt (h) is the discharging time.

The chemical diffusion coefficient of k^+ can be calculated based on the following equation:

$$D_{GITT} = \frac{4}{\pi\tau}\left(\frac{n_m V_m}{s}\right)^2\left(\frac{\Delta E_s}{\Delta E_t}\right)^2 \tag{4}$$

Here, τ (s) is the duration of the current pulse; n_m (mol) is the number of moles; V_m (cm^3 mol^{-1}) is the molar volume of the electrode; S (cm^2) is the electrode/electrolyte contact area; ΔE_s is the steady state voltage change due to the current pulse, and ΔE_t is the voltage change during the constant current pulse, eliminating the iR drop.

Figure S1. NP-3DPG powder on an evaporating dish.

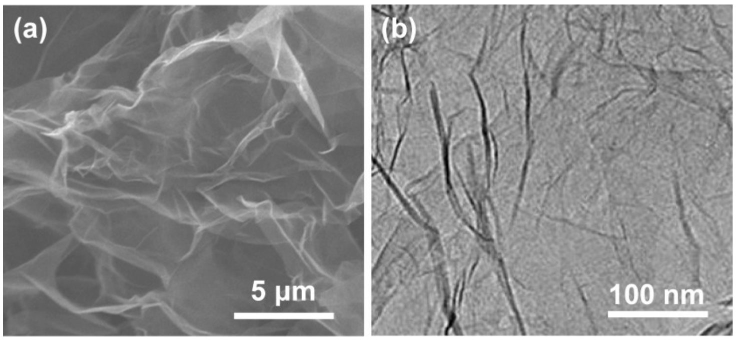

Figure S2. (a) SEM and (b) TEM of GO.

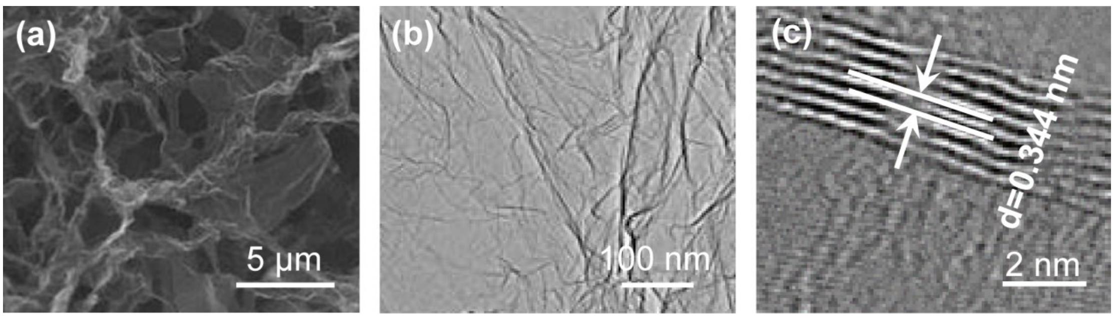

Figure S3. (a) SEM, (b) TEM, and (C) HRTEM of N-3DPG.

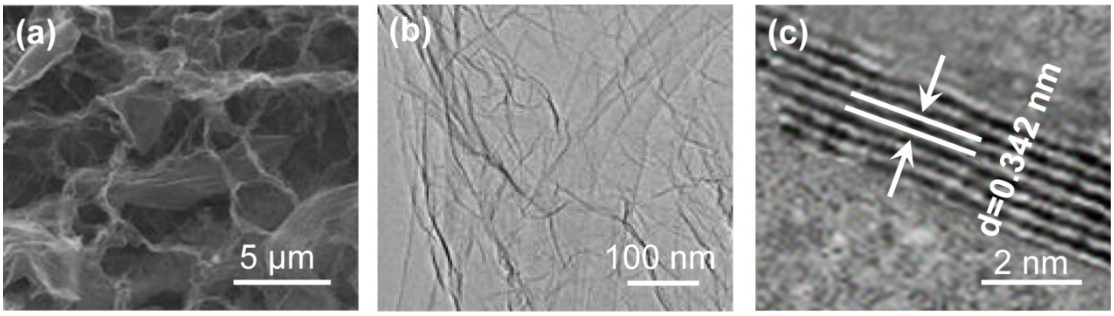

Figure S4. (a) SEM, (b) TEM, and (C) HRTEM of 3DPG.

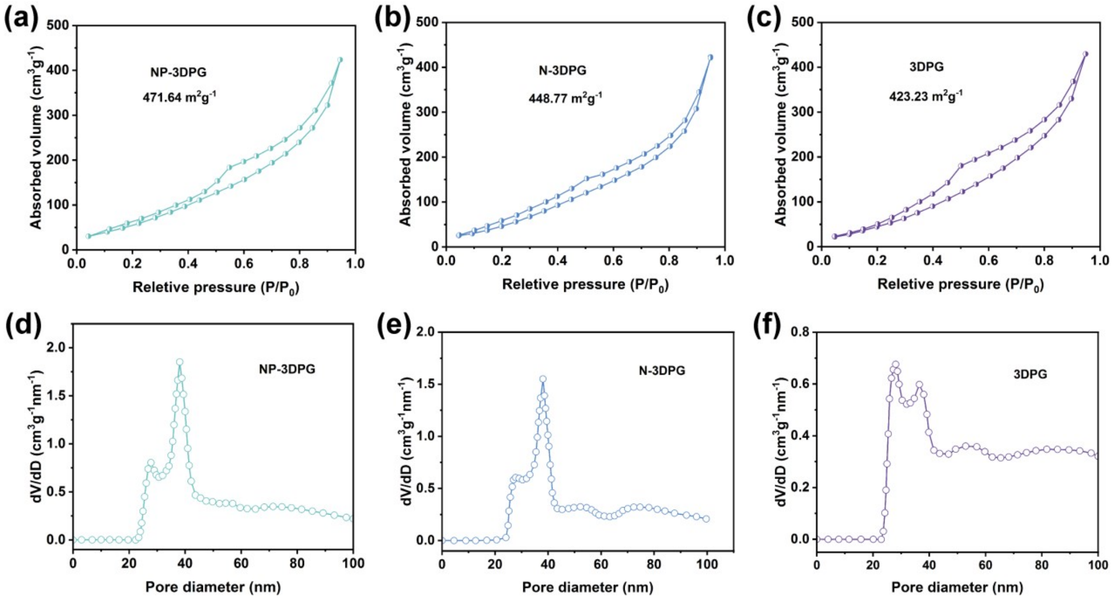

Figure S5. Nitrogen adsorption–desorption isotherm of (a) NP-3DPG, (b) N-3DPG, and (c) 3DPG. Pore size distribution of (d) NP-3DPG, (e) N-3DPG, and (f) 3DPG.

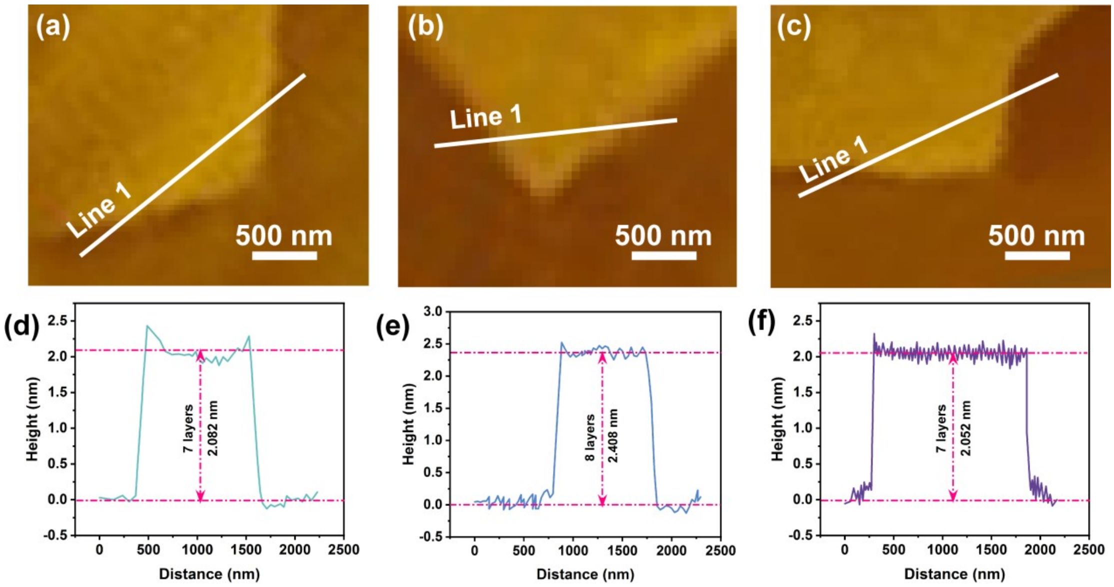

Figure S6. AFM images of (a) NP-3DPG, (a) N-3DPG, and (c) 3DPG. Height profiles of (d) NP-3DPG, (e) N-3DPG, and (f) 3DPG.

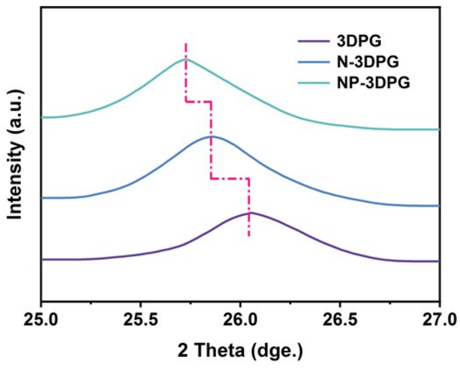

Figure S7. Partial enlarged XRD patterns of 3DPG, N-3DPG and NP-3DPG.

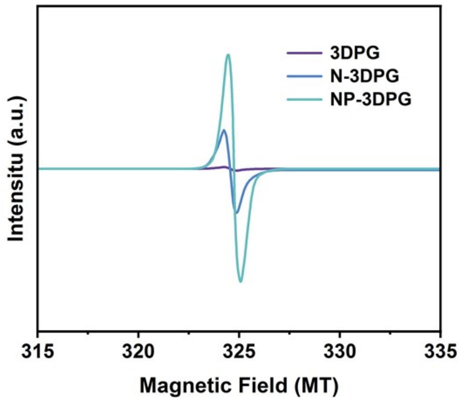

Figure S8. EPR spectra of NP-3DPG, N-3DPG and 3DPG.

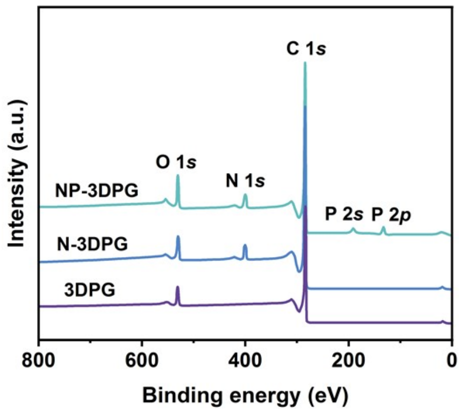

Figure S9. XPS survey spectrum of 3DPG, N-3DPG, and NP-3DPG.

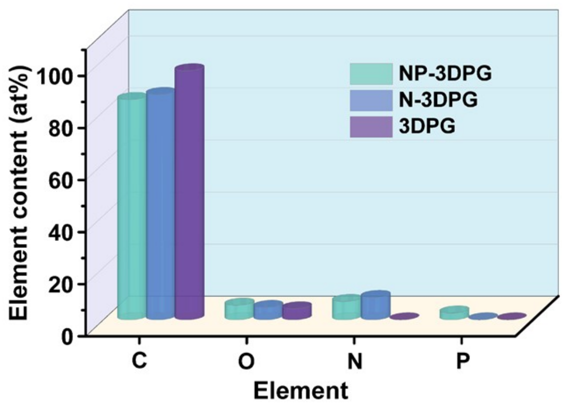

Figure S10. Element content of 3DPG, N-3DPG, and NP-3DPG.

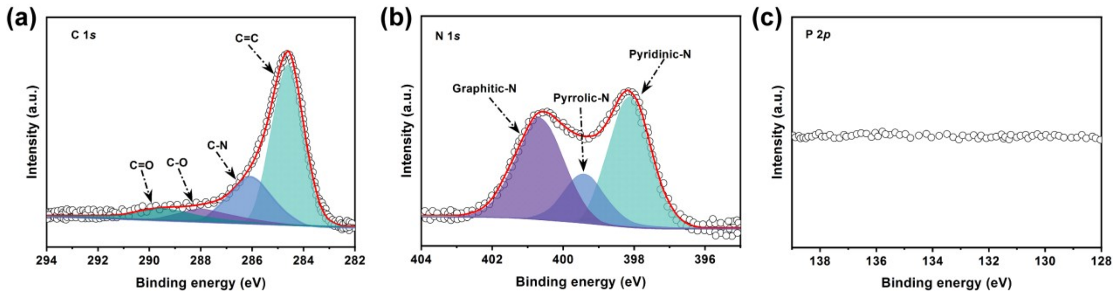

Figure S11. (a) C 1*s*, (b) N 1*s*, and (c) P 2*p* high-resolution XPS of N-3DPG.

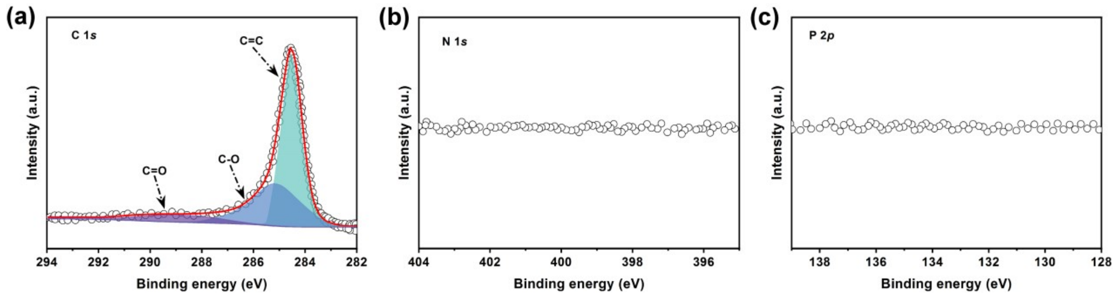

Figure S12. (a) C 1*s*, (b) N 1*s*, and (c) P 2*p* high-resolution XPS of 3DPG.

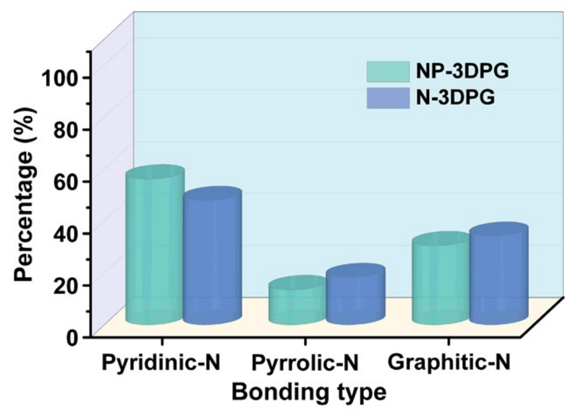

Figure S13. Percentage contents of nitrogen species in the N-3DPG and NP-3DPG.

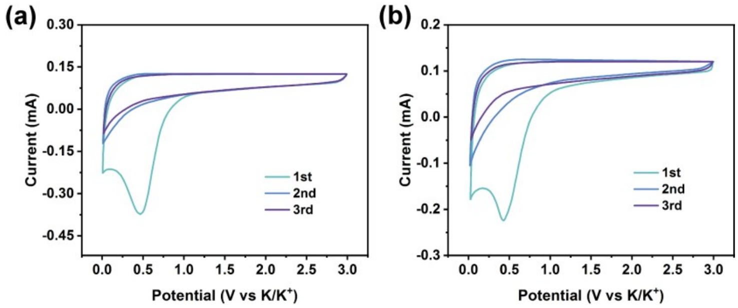

Figure S14. CV curves of (a) N-3DPG and (b) 3DPG electrode.

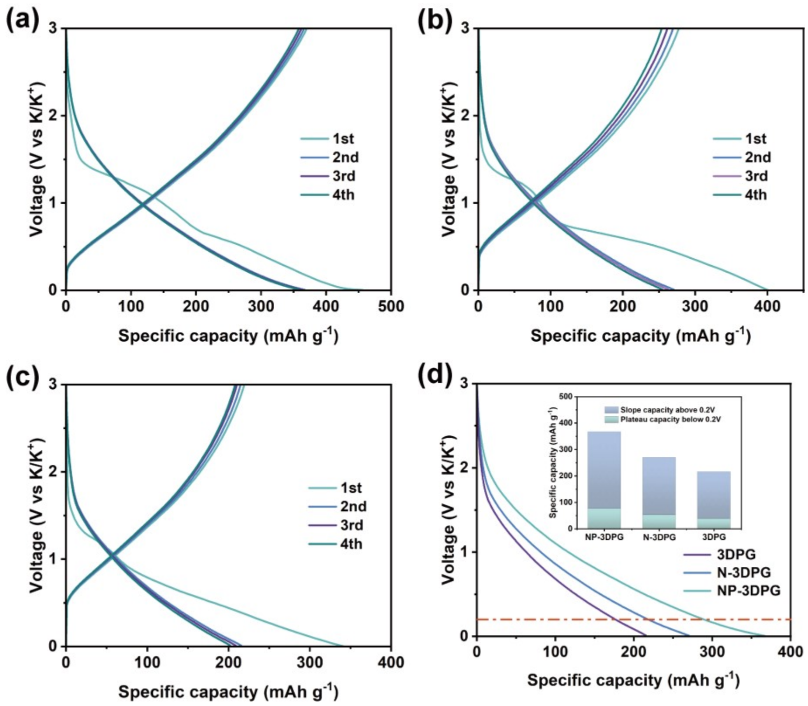

Figure S15. GCD profiles of the (a) NP-3DPG, (b) N-3DPG and (c) 3DPG electrodes at 0.2 A g^{-1}. (d) The discharge profiles of NP-3DPG, N-3DPG and 3DPG at second cycle (inset: the capacity contribution at each stage).

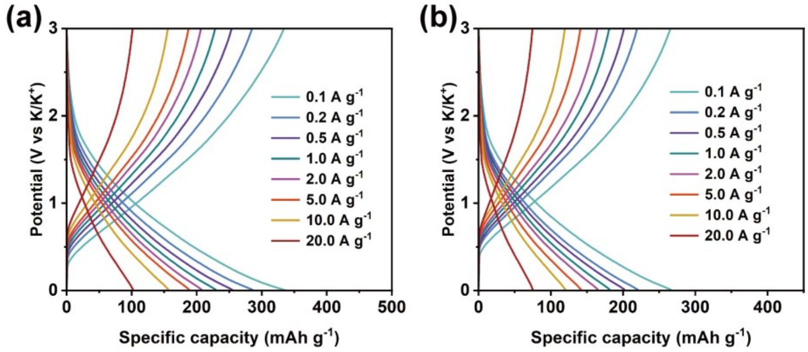

Figure S16. GCD curves at various current densities for (a) N-3DPG and (b) 3DPG.

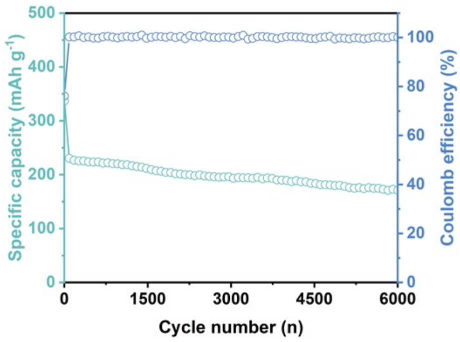

Figure S17. Long-term cycling performance of the NP-3DG at 5.0 A g^{-1}.

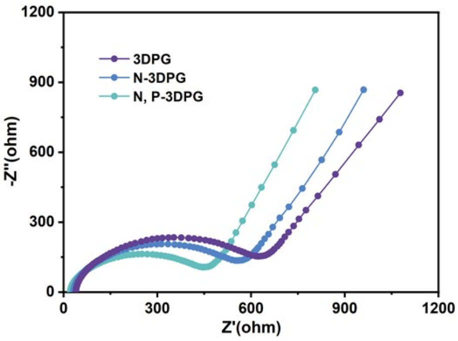

Figure S18. Electrochemical impedance spectra (EIS) of the 3DPG, N-3DPG and NP-3DPG electrodes.

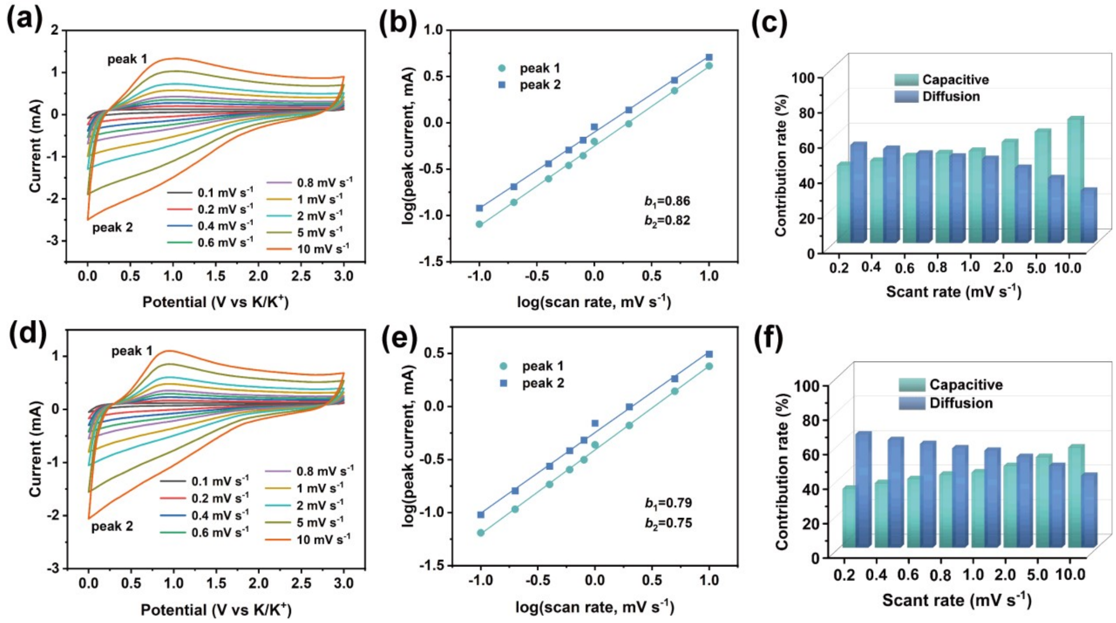

Figure S19. CV curves of (a) N-3DPG and (d) 3DPG. *b*-value of (b) N-3DPG and (d) 3DPG. Diffusive and capacitive contributions of (c) N-3DPG and (f) 3DPG.

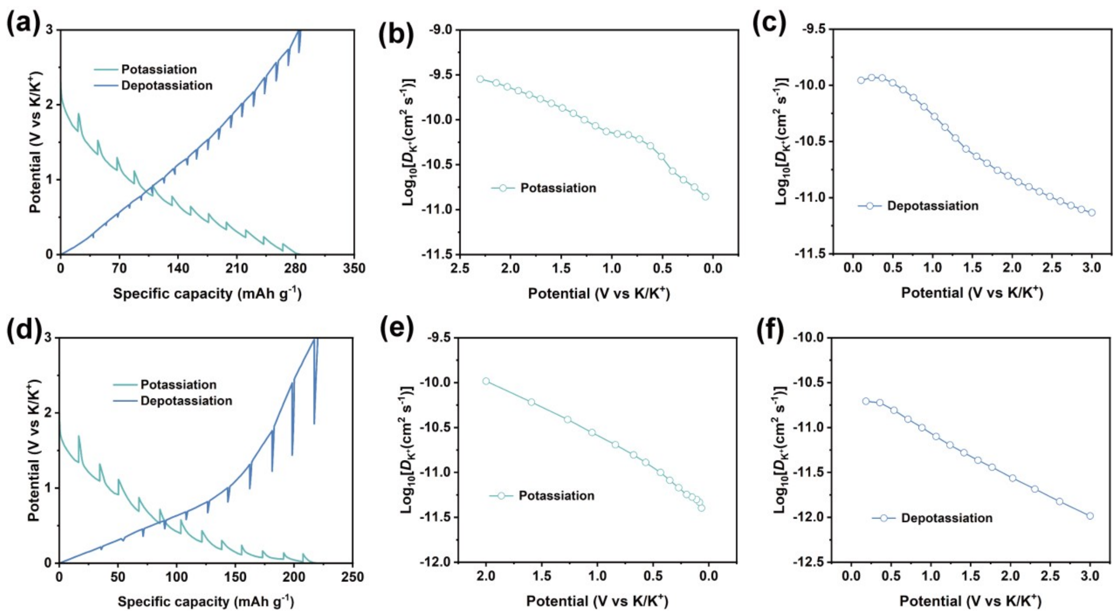

Figure S20. GITT profiles of (a) N-3DPG and (d) 3DPG; Potassiation D_k of (b) N-3DPG and (e) 3DPG; and depotassiation D_k of (c) N-3DPG and (f) 3DPG.

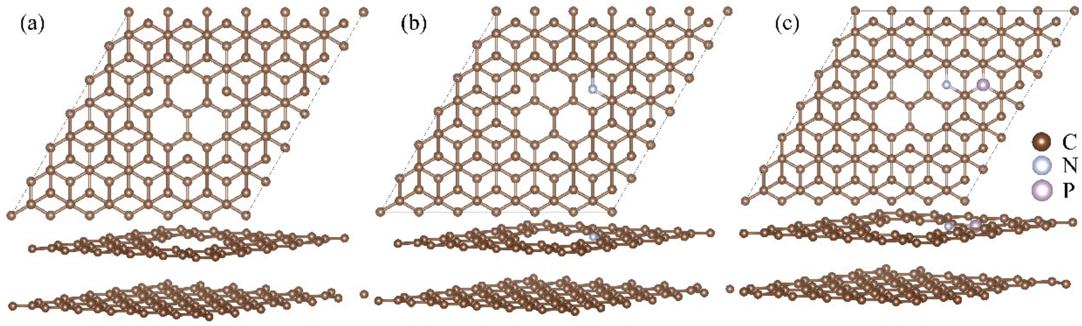

Figure S21. Top and side view of the optimized structure of (a) 3DPG, (b) N-3DPG and (c) NP-3DPG.

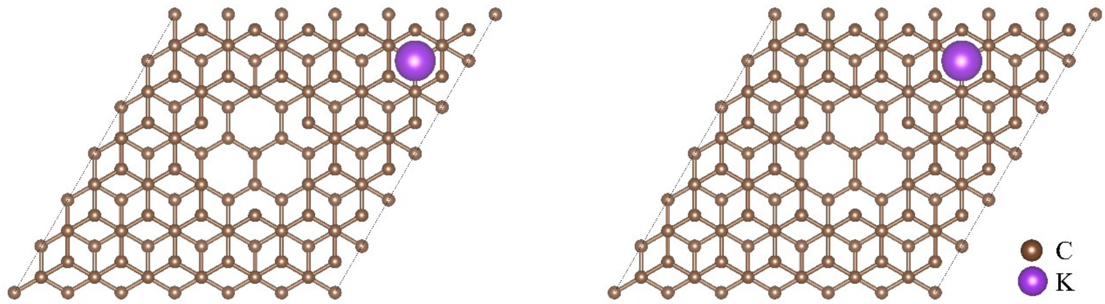

Figure S22. Illustration of the K ion diffusion path from one hollow position to the nearest hollow position in 3DPG.

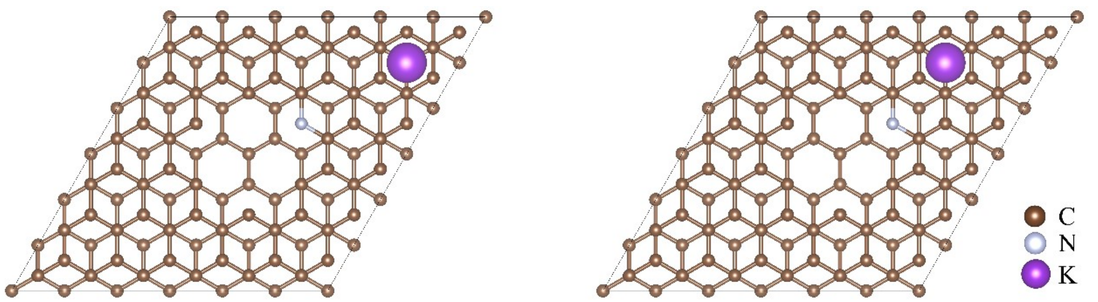

Figure S23. Illustration of the K ion diffusion path from one hollow position to the nearest hollow position in N-3DPG.

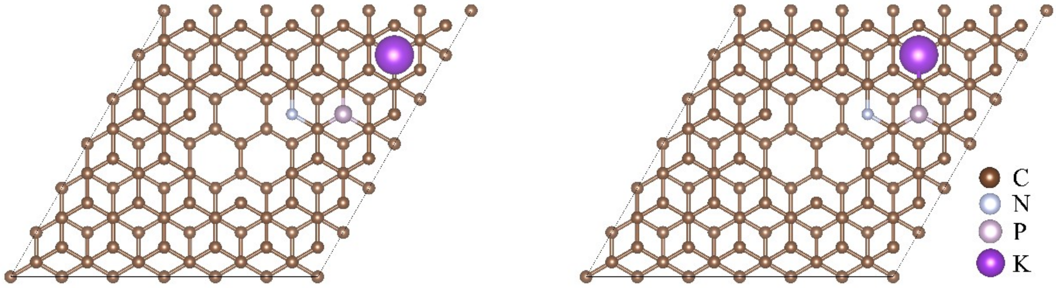

Figure S24. Illustration of the K ion diffusion path from one hollow position to the nearest hollow position in NP-3DPG.

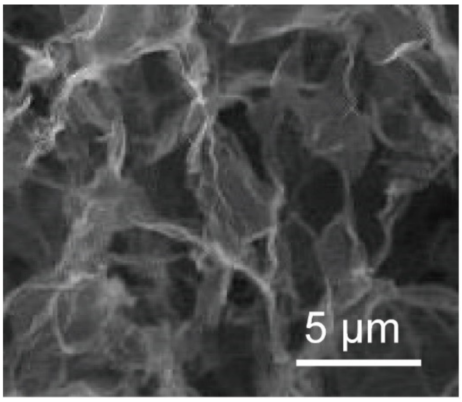

Figure S25. SEM of ANP-3DPG.

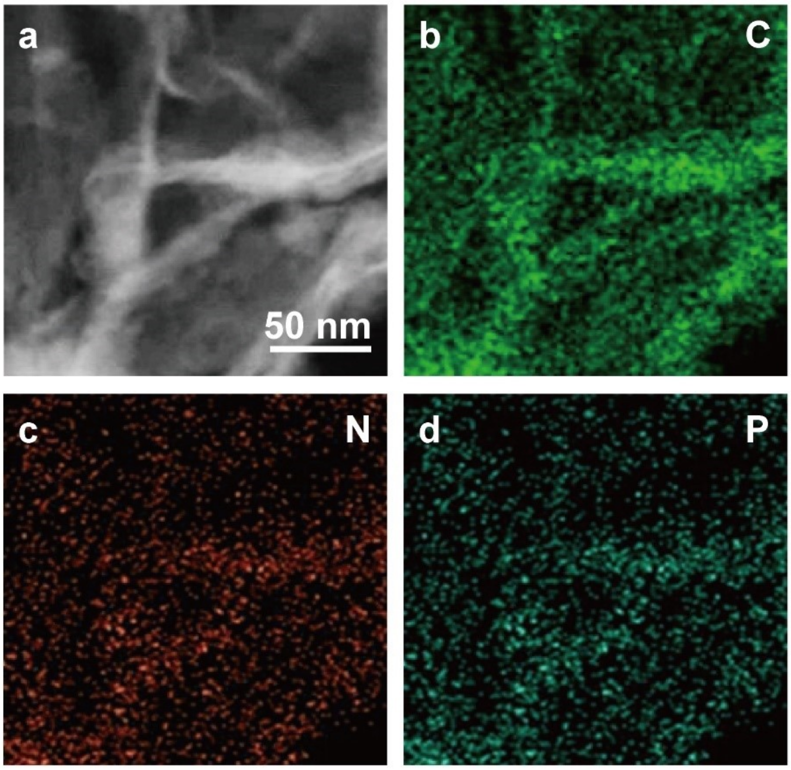

Figure S26. (a) STEM image, (b) C, (c) N, and (d) P elemental mapping of ANP-3DPG.

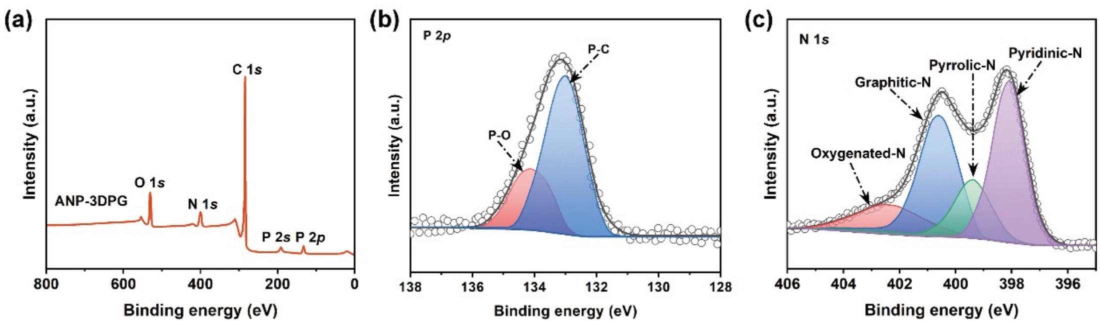

Figure S27. (a) The survey XPS spectrum, (b) high-resolution P 2*p* spectra, (c) high-resolution N 1*s* spectra of ANP-3DPG.

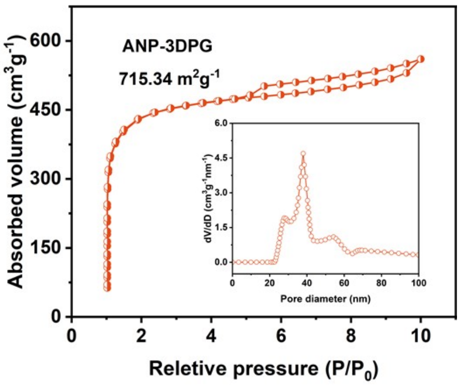

Figure S28. Nitrogen adsorption–desorption isotherm of ANP-3DPG.

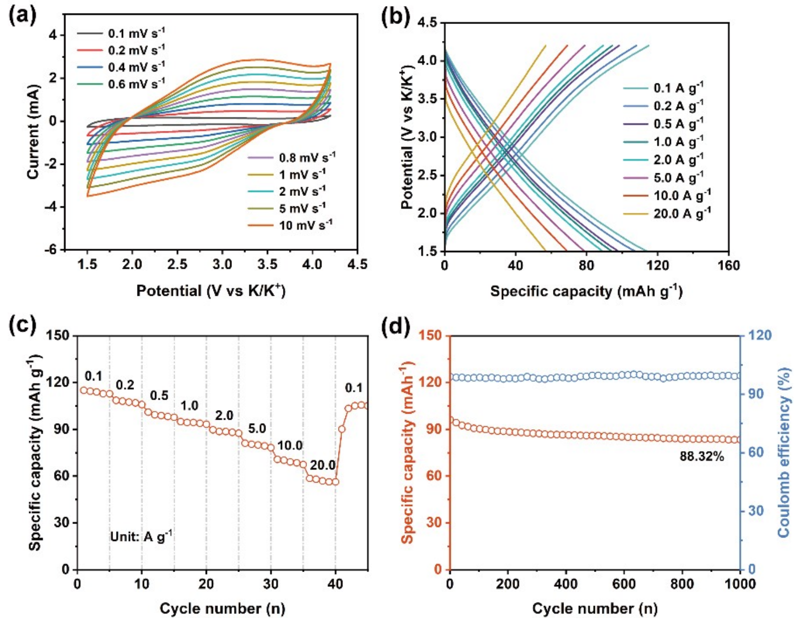

Figure S29. Electrochemical performances of the ANP-3DPG cathode in K-half cells. (a) CV curves at different scan rates, (b) charge/discharge curves at various current densities, (c) rate property, and (g) cycling performance at 1.0 A g^{-1}.

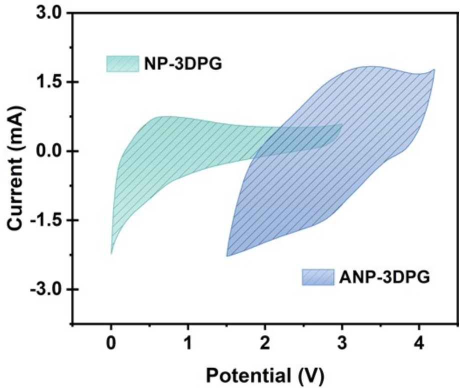

Figure S30. CV curves of the NP-3DPG and the ANP-3DPG electrodes in half cells at 1 mV s^{-1}.

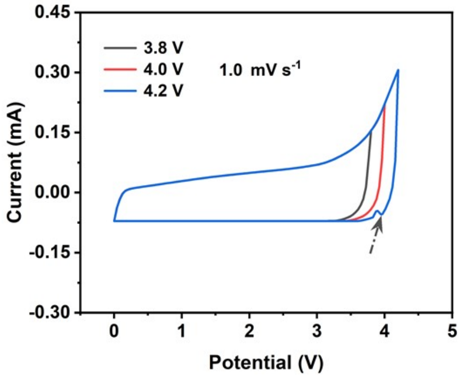

Figure S31. CV curves of ANP-3DPG//NP-3DPG PIHCs device in different potential windows at a scan rate of 1.0 mV s^{-1}.

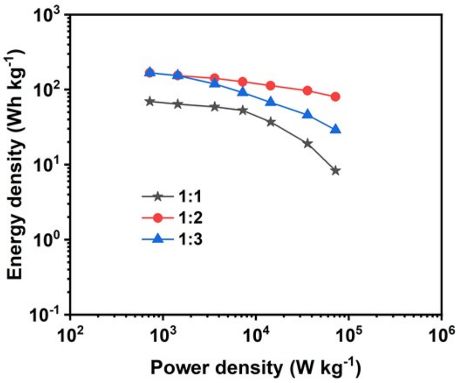

Figure S32. Ragone plots of NP-3DPG//ANP-3DPG PIHCs device with different mass ratios of anode to cathode.

Table S1. Comparison of the initial coulombic efficiency of the carbonaceous electrodes for PIBs with our work.

Materials	**Current density ($A\ g^{-1}$)**	**Initial coulombic efficiency**	**Reference**
NP-3DPG	0.2	81.4%	This work
PN-HPCNF	0.2	78.9%	[1]
PDDA-NPCNs/Ti_3C_2	0.1	73.2%	[2]
nitrogen/oxygen codoped carbon hollow multihole bowls	0.1	63.3%	[3]
oxygen/fluorine dualdoped porous carbon	0.1	63%	[4]

S/O codoped porous carbon microspheres	0.05	61.7%	[5]
mesoporous graphitic carbon nanospring	0.05	61.2%	[6]
P-doped N-rich honeycomb-like carbon	0.2	56.9%	[7]
Sulfur-grafted hollow carbon spheres	0.025	51.4%	[8]
N-doped carbon nanofibers-650	0.025	49%	[9]
N/O dual-doped carbon network	0.05	47.12%	[10]
P-doped hard carbon	0.1	45.7%	[11]
rGO aerogel	0.1	44%	[12]
nitrogen-doped porous carbon	0.1	43.1%	[13]
graphitic carbon nanocage	0.05	40%	[14]
carbon nanosheets750	0.05	38%	[15]
nitrogen/oxygen in situ dual-doped hierarchical porous hard carbon	0.05	25%	[16]
S/N@C	0.05	24.6%	[17]

three-dimensional nitrogen-doped framework carbon	0.1	24.3%	[18]
NHC_2-NH_3/Ar	0.1	15.8%	[19]
Hierarchical carbon nanotube-S4	0.1	15%	[20]
pyridinic N-contentdoped porous carbon monolith	0.02	10%	[21]

Table S2. Potassium storage performance of NP-3DPG compared with previously reported materials.

Materials	**Rate capacity**	**Cycling stability**	**Ref.**
NP-3DPG	429.5 mA h g^{-1} at 20.0 A g^{-1}	236.5 mA h g^{-1} after 15000 cycles at 5.0 A g^{-1}	This work
Nitrogen doped cup-stacked carbon tubes	75 mA h g^{-1} at 1 A g^{-1}	236 mA h g^{-1} after 100 cycles at 0.02 A g^{-1}	[22]
High pyridine N-doped porous carbon	182.6 mAh g^{-1} at 2 A g^{-1}	231.6 mAh g^{-1} after 200 cycles at 0.5 A g^{-1}	[23]
Co_3O_4–Fe_2O_3/C	278 mAh g^{-1} at 1 A	220 mAh g^{-1} after 50 cycles	[24]

	g^{-1}	at 0.05 A g^{-1}	
Hyperporous carbon sponge	180 mAh g^{-1} at 1.6 A g^{-1}	210 mAh g^{-1} after 500 cycles at 1 A g^{-1}	[20]
Nitrogen-doped bamboo-like carbon nanotubes	186 mAh g^{-1} at 1 A g^{-1}	204 mAh g^{-1} after 1000 cycles at 0.5 A g^{-1}	[25]
Chemically activated hollow carbon nanospheres	137 mA h g^{-1} at 4A g^{-1}	192.7 mAh g^{-1} after 5000 cycles at 2 A g^{-1}	[26]
Sulfur/nitrogen codoped carbon nanofiber agerogel	168 mA h g^{-1} at 2 A g^{-1}	168 mA h g^{-1} after 1000 cycles at 2 A g^{-1}	[27]
Hollow carbon architecture	110 mAh g^{-1} at 0.56 A g^{-1}	150 mA h g^{-1} after 500 cycles at 0.279 A g^{-1}	[28]
Nitrogen doped carbon nanofibers	153 mA h g^{-1} at 2 A g^{-1}	146 mA h g^{-1} after 4000 cycles at 2 A g^{-1}	[9]
S-NC	72 mA h g^{-1} at 10 A g^{-1}	140 mA h g^{-1} after 3000 cycles at 2 A g^{-1}	[29]
3D nitrogen-doped framework carbon	111 mA h g^{-1} at 10 A g^{-1}	137 mA h g^{-1} after 1000 cycles at 2 A g^{-1}	[18]
N-doped carbon	102.6 mA h g^{-1} at 2 A g^{-1}	119.9 mA h g^{-1} after 1000 cycles at 1 A g^{-1}	[30]

Oxygen-Rich Carbon Nanosheets	133 mA h g^{-1} at 10 A g^{-1}	111 mA h g^{-1} after 3000 cycles at 5 A g^{-1}	[15]
Onion-like carbon	78 mA h g^{-1} at 10 A g^{-1}	111 mA h g^{-1} after 1000 cycles at 2 A g^{-1}	[31]
Sulfur/oxygen co-doped hard carbon	158 mAh g^{-1} at 1 A g^{-1}	108.4 mA h g^{-1} after 2000 cycles at 1 A g^{-1}	[5]
Nitrogen-doped carbon nanotubes	102 mA h g^{-1} at 2 A g^{-1}	102 mA h g^{-1} after 500 cycles at 2 A g^{-1}	[32]
Hierarchically Porous Thin Carbon Shells	64 mA h g^{-1} at 4 A g^{-1}	65 mA h g^{-1} after 900 cycles at 2 A g^{-1}	[17]

Table S3. The comparison between NP-3DPG//ANP-3DPG PIHCs and other recently reported carbonaceous based PIHCs.

Devices	**Maximum Energy density (Wh kg^{-1})/Power density (W kg^{-1})**	**Maximum Power density (W kg^{-1})/Energy density (Wh kg^{-1})**	**Cycles /Capacity retention (%)/current (A g^{-1})**	**Ref.**
MoP@NC-1//AC	69.7/100	2041.6/20	800/89.9/0.1	[33]

CTP@C//AC	80/32	5144/34	1000/75.9/5	[34]
NOHPC//HPAC	90.1/939.6	6217.5/52.93	6000/87.2/2	[35]
BSH//AC	94/188	599/13.3	1000/71.4/0.34	[36]
PNC//HPC	103/97.9	6106.2/44.1	5000/64/1	[37]
WS_2@NCNs//NCHS	103.4/235	2300/60	500/78/0.5	[38]
NHCS//ANHCS	114.2/100.5	8203/19.1	5000/80.4/2	[39]
NCNT//AC	115/116.8	1713.4/25.7	2000/81.6/1	[40]
N-$MoSe_2$/G//AC	119/39.6	7212/29	3000/75.2/1	[41]
N,S-3DHPC-600//AC-800	130.6/210	16800/56	5000/86.8/5	[42]
$NbSe_2$/NSeCNFs//AC	133/180	4000/18	10000/83/2	[43]
SHPNC//AC	135/112.6	~4000/20	3750/75.4/1	[44]
PN-PanC//PN-PanC	155.9/76.1	11309.1/22.0	40000/77/1	[45]
M-NC/ANC	157/37	2300/49	3000/80//0.5	[46]
P/O-PCS//AC	158/223	1380/11	30000/94.5/5	[47]
3DNFC//3DNFAC	163.5/210	21000/76.4	10000/91.7/2	[18]
NP-3DPG//ANP-3DPG	167.4/720	72000/80.2	10000/87.3/2	This work

References

[1] X. Hu, G. Zhong, J. Li, Y. Liu, J. Yuan, J. Chen, H. Zhan, Z. Wen, Hierarchical porous carbon nanofibers for compatible anode and cathode of potassium-ion hybrid capacitor, Energy & Environmental Science, 13 (2020) 2431-2440.

[2] R. Zhao, H. Di, X. Hui, D. Zhao, R. Wang, C. Wang, L. Yin, Self-assembled Ti 3 C 2 MXene and N-rich porous carbon hybrids as superior anodes for high-performance potassium-ion batteries, Energy & Environmental Science, 13 (2020) 246-257.

[3] Z. Zhang, B. Jia, L. Liu, Y. Zhao, H. Wu, M. Qin, K. Han, W.A. Wang, K. Xi, L. Zhang, Hollow multihole carbon bowls: A stress–release structure design for high-stability and high-volumetric-capacity potassium-ion batteries, ACS nano, 13 (2019) 11363-11371.

[4] J. Lu, C. Wang, H. Yu, S. Gong, G. Xia, P. Jiang, P. Xu, K. Yang, Q. Chen, Oxygen/fluorine dual-doped porous carbon nanopolyhedra enabled ultrafast and highly stable potassium storage, Advanced Functional Materials, 29 (2019) 1906126.

[5] M. Chen, W. Wang, X. Liang, S. Gong, J. Liu, Q. Wang, S. Guo, H. Yang, Sulfur/oxygen codoped porous hard carbon microspheres for high-performance potassium-ion batteries, Advanced Energy Materials, 8 (2018) 1800171.

[6] Y. Qian, S. Jiang, Y. Li, Z. Yi, J. Zhou, J. Tian, N. Lin, Y. Qian, Water-induced growth of a highly oriented mesoporous graphitic carbon nanospring for fast potassium-ion adsorption/intercalation storage, Angewandte Chemie International Edition, 58 (2019) 18108-18115.

[7] H. He, D. Huang, Y. Tang, Q. Wang, X. Ji, H. Wang, Z. Guo, Tuning nitrogen species in three-dimensional porous carbon via phosphorus doping for ultra-fast potassium storage, Nano Energy, 57 (2019) 728-736.

[8] J. Ding, H. Zhang, H. Zhou, J. Feng, X. Zheng, C. Zhong, E. Paek, W. Hu, D. Mitlin, Sulfur-grafted hollow carbon spheres for potassium-ion battery anodes, Advanced Materials, 31 (2019) 1900429.

[9] Y. Xu, C. Zhang, M. Zhou, Q. Fu, C. Zhao, M. Wu, Y. Lei, Highly nitrogen doped carbon nanofibers with superior rate capability and cyclability for potassium ion batteries, Nature communications, 9 (2018) 1720.

[10] J. Ruan, Y. Zhao, S. Luo, T. Yuan, J. Yang, D. Sun, S. Zheng, Fast and stable potassium-ion storage achieved by in situ molecular self-assembling N/O dual-doped carbon network, Energy Storage Materials, 23 (2019) 46-54.

[11] Y. Qian, S. Jiang, Y. Li, Z. Yi, J. Zhou, T. Li, Y. Han, Y. Wang, J. Tian, N. Lin, In Situ Revealing the Electroactivity of P□ O and P□ C Bonds in Hard Carbon for High-Capacity and Long-Life Li/K-Ion Batteries, Advanced Energy Materials, 9 (2019) 1901676.

[12] L. Liu, Z. Lin, J.-Y. Chane-Ching, H. Shao, P.-L. Taberna, P. Simon, 3D rGO aerogel with superior electrochemical performance for K–Ion battery, Energy Storage Materials, 19 (2019) 306-313.

[13] D. Li, X. Ren, Q. Ai, Q. Sun, L. Zhu, Y. Liu, Z. Liang, R. Peng, P. Si, J. Lou, Facile fabrication of nitrogen-doped porous carbon as superior anode material for potassium-ion batteries, Advanced Energy Materials, 8 (2018) 1802386.

[14] B. Cao, Q. Zhang, H. Liu, B. Xu, S. Zhang, T. Zhou, J. Mao, W.K. Pang, Z. Guo, A. Li, Graphitic carbon nanocage as a stable and high power anode for potassium-ion batteries, Advanced Energy Materials, 8 (2018) 1801149.

[15] J. Chen, B. Yang, H. Hou, H. Li, L. Liu, L. Zhang, X. Yan, Disordered, large interlayer spacing, and oxygen-rich carbon nanosheets for potassium ion hybrid capacitor, Advanced Energy Materials, 9 (2019) 1803894.

[16] J. Yang, Z. Ju, Y. Jiang, Z. Xing, B. Xi, J. Feng, S. Xiong, Enhanced capacity and rate capability of nitrogen/oxygen dual-doped hard carbon in capacitive potassium-ion storage, Advanced Materials, 30 (2018) 1700104.

[17] A. Mahmood, S. Li, Z. Ali, H. Tabassum, B. Zhu, Z. Liang, W. Meng, W. Aftab, W. Guo, H. Zhang, Ultrafast sodium/potassium-ion intercalation into hierarchically porous thin carbon shells, Advanced Materials, 31 (2019) 1805430.

[18] B. Yang, J. Chen, L. Liu, P. Ma, B. Liu, J. Lang, Y. Tang, X. Yan, 3D nitrogen-doped framework carbon for high-performance potassium ion hybrid capacitor, Energy Storage Materials, 23 (2019) 522-529.

[19] W. Yang, J. Zhou, S. Wang, W. Zhang, Z. Wang, F. Lv, K. Wang, Q. Sun, S. Guo, Freestanding film made by necklace-like N-doped hollow carbon with hierarchical pores for high-performance potassium-ion storage, Energy & Environmental Science, 12 (2019) 1605-1612.

[20] Y. Wang, Z. Wang, Y. Chen, H. Zhang, M. Yousaf, H. Wu, M. Zou, A. Cao, R.P. Han, Hyperporous sponge interconnected by hierarchical carbon nanotubes as a high-performance potassium-ion battery anode, Advanced Materials, 30 (2018)

1802074.

[21] Y. Xie, Y. Chen, L. Liu, P. Tao, M. Fan, N. Xu, X. Shen, C. Yan, Ultra-high pyridinic N-doped porous carbon monolith enabling high-capacity K-ion battery anodes for both half-cell and full-cell applications, Advanced Materials, 29 (2017) 1702268.

[22] X. Zhao, Y. Tang, C. Ni, J. Wang, A. Star, Y. Xu, Free-standing nitrogen-doped cup-stacked carbon nanotube mats for potassium-ion battery anodes, ACS Applied Energy Materials, 1 (2018) 1703-1707.

[23] Y. Li, C. Yang, F. Zheng, X. Ou, Q. Pan, Y. Liu, G. Wang, High pyridine N-doped porous carbon derived from metal–organic frameworks for boosting potassium-ion storage, Journal of Materials Chemistry A, 6 (2018) 17959-17966.

[24] I. Sultana, M.M. Rahman, S. Mateti, V.G. Ahmadabadi, A.M. Glushenkov, Y. Chen, K-ion and Na-ion storage performances of Co 3 O 4–Fe 2 O 3 nanoparticle-decorated super P carbon black prepared by a ball milling process, Nanoscale, 9 (2017) 3646-3654.

[25] Y. Liu, C. Yang, Q. Pan, Y. Li, G. Wang, X. Ou, F. Zheng, X. Xiong, M. Liu, Q. Zhang, Nitrogen-doped bamboo-like carbon nanotubes as anode material for high performance potassium ion batteries, Journal of Materials Chemistry A, 6 (2018) 15162-15169.

[26] G. Wang, X. Xiong, D. Xie, Z. Lin, J. Zheng, F. Zheng, Y. Li, Y. Liu, C. Yang, M. Liu, Chemically activated hollow carbon nanospheres as a high-performance anode material for potassium ion batteries, Journal of Materials Chemistry A, 6 (2018)

24317-24323.

[27] C. Lv, W. Xu, H. Liu, L. Zhang, S. Chen, X. Yang, X. Xu, D. Yang, 3D sulfur and nitrogen codoped carbon nanofiber aerogels with optimized electronic structure and enlarged interlayer spacing boost potassium-ion storage, Small, 15 (2019) 1900816.

[28] W. Wang, J. Zhou, Z. Wang, L. Zhao, P. Li, Y. Yang, C. Yang, H. Huang, S. Guo, Short-range order in mesoporous carbon boosts potassium-ion battery performance, Advanced Energy Materials, 8 (2018) 1701648.

[29] L. Tao, Y. Yang, H. Wang, Y. Zheng, H. Hao, W. Song, J. Shi, M. Huang, D. Mitlin, Sulfur-nitrogen rich carbon as stable high capacity potassium ion battery anode: Performance and storage mechanisms, Energy Storage Materials, 27 (2020) 212-225.

[30] C. Gao, Q. Wang, S. Luo, Z. Wang, Y. Zhang, Y. Liu, A. Hao, R. Guo, High performance potassium-ion battery anode based on biomorphic N-doped carbon derived from walnut septum, Journal of power sources, 415 (2019) 165-171.

[31] J. Chen, B. Yang, H. Li, P. Ma, J. Lang, X. Yan, Candle soot: onion-like carbon, an advanced anode material for a potassium-ion hybrid capacitor, Journal of Materials Chemistry A, 7 (2019) 9247-9252.

[32] P. Xiong, X. Zhao, Y. Xu, Nitrogen-doped carbon nanotubes derived from metal–organic frameworks for potassium-ion battery anodes, ChemSusChem, 11 (2018) 202-208.

[33] W. Zong, N. Chui, Z. Tian, Y. Li, C. Yang, D. Rao, W. Wang, J. Huang, J. Wang,

F. Lai, Ultrafine MoP nanoparticle splotched nitrogen-doped carbon nanosheets enabling high-performance 3D-printed potassium-ion hybrid capacitors, Advanced Science, 8 (2021) 2004142.

[34] Z. Zhang, M. Li, Y. Gao, Z. Wei, M. Zhang, C. Wang, Y. Zeng, B. Zou, G. Chen, F. Du, Fast potassium storage in hierarchical Ca0. 5Ti2 (PO4) 3@ C microspheres enabling high-performance potassium-ion capacitors, Advanced Functional Materials, 28 (2018) 1802684.

[35] Z. Pan, Y. Qian, Y. Li, X. Xie, N. Lin, Y. Qian, Novel bilayer-shelled N, O-doped hollow porous carbon microspheres as high performance anode for potassium-ion hybrid capacitors, Nano-Micro Letters, 15 (2023) 151.

[36] L. Fan, K. Lin, J. Wang, R. Ma, B. Lu, A nonaqueous potassium-based battery–supercapacitor hybrid device, Advanced materials, 30 (2018) 1800804.

[37] Z. Xie, J. Xia, D. Qiu, J. Wei, M. Li, F. Wang, R. Yang, Rich-phosphorus/nitrogen co-doped carbon for boosting the kinetics of potassium-ion hybrid capacitors, Sustainable Energy & Fuels, 6 (2022) 162-169.

[38] Y. Li, Y. Yang, P. Zhou, T. Gao, Z. Xu, S. Lin, H. Chen, J. Zhou, S. Guo, Enhanced cathode and anode compatibility for boosting both energy and power densities of Na/K-ion hybrid capacitors, Matter, 1 (2019) 893-910.

[39] D. Qiu, J. Guan, M. Li, C. Kang, J. Wei, Y. Li, Z. Xie, F. Wang, R. Yang, Kinetics enhanced nitrogen-doped hierarchical porous hollow carbon spheres boosting advanced potassium-ion hybrid capacitors, Advanced Functional Materials, 29 (2019) 1903496.

[40] X. Li, M. Chen, L. Wang, H. Xu, J. Zhong, M. Zhang, Y. Wang, Q. Zhang, L. Mei, T. Wang, Nitrogen-doped carbon nanotubes as an anode for a highly robust potassium-ion hybrid capacitor, Nanoscale Horizons, 5 (2020) 1586-1595.

[41] Y. Yi, Z. Sun, C. Li, Z. Tian, C. Lu, Y. Shao, J. Li, J. Sun, Z. Liu, Designing 3D biomorphic nitrogen-doped MoSe2/graphene composites toward high-performance potassium-ion capacitors, Advanced Functional Materials, 30 (2020) 1903878.

[42] B. Fan, J. Yan, A. Hu, Z. Liu, W. Li, Y. Li, Y. Xu, Y. Zhang, Q. Tang, X. Chen, High-performance potassium ion capacitors enabled by hierarchical porous, large interlayer spacing, active site rich-nitrogen, and sulfur Co-doped carbon, Carbon, 164 (2020) 1-11.

[43] M. Chen, L. Wang, X. Sheng, T. Wang, J. Zhou, S. Li, X. Shen, M. Zhang, Q. Zhang, X. Yu, An ultrastable nonaqueous potassium-ion hybrid capacitor, Advanced Functional Materials, 30 (2020) 2004247.

[44] H. Luo, M. Chen, J. Cao, M. Zhang, S. Tan, L. Wang, J. Zhong, H. Deng, J. Zhu, B. Lu, Hierarchically Porous Carbon as Anode for Highly Robust Potassium-Ion Hybrid Capacitors, Nano-Micro Lett, 12 (2020) 113.

[45] G. Wang, W. Wang, X. He, J. Li, L. Yu, B. Peng, G. Zhang, Concunrent manipulation of anion and cation adsorption kinetics in pancake-like carbon achieves ultrastable potassium ion hybrid capacitors, Energy Storage Materials, 46 (2022) 10-19.

[46] Y. Yi, Z. Zeng, X. Lian, S. Dou, J. Sun, Homologous Nitrogen-Doped Hierarchical Carbon Architectures Enabling Compatible Anode and Cathode for

Potassium-Ion Hybrid Capacitors, Small, 18 (2022) 2107139.

[47] S. Zhao, K. Yan, J. Liang, Q. Yuan, J. Zhang, B. Sun, P. Munroe, G. Wang, Phosphorus and oxygen dual-doped porous carbon spheres with enhanced reaction kinetics as anode materials for high-performance potassium-ion hybrid capacitors, Advanced Functional Materials, 31 (2021) 2102060.